Theoretical Analysis of Control Properties for the Brushless Doubly-Fed Reluctance Machine

R.E. Betz *Member, IEEE* and M.G. Jovanović *Member, IEEE*

Abstract— **The brushless doubly-fed induction machine (BDFIM) has been extensively researched over approximately 30 years, but a related machine, the brushless doubly fed reluctance machine (BDFRM), has not. This was mainly due to the fact that reluctance rotor designs were not capable of generating saliency ratios large enough to make the BDFRM competitive with other machines. However recent developments in reluctance rotors, spurred on by research into synchronous reluctance machines, has resulted in high saliency ratio rotors that are economic to build. This, together with the promise of higher efficiency and simpler control compared to the BDFIM, means that further investigation of the BDFRM is warranted. A relatively limited amount of work to date has been published on the BDFRM. This paper attempts to fill this void by presenting a theoretical analysis of some of the important control properties of the ideal BDFRM.**

Keywords— **brushless doubly-fed machine, self cascade machine, reluctance machine, electric machine control.**

I. Introduction

THE Brushless Doubly Fed Reluctance Machine (BDFRM) belongs to a group of interesting machines that include the classical cascaded induction machine (CIM), the traditional double fed slip ring induction machine (DFSRIM), and the Brushless Doubly Fed Induction Machine (BDFIM).

The CIM, which forms the philosophical basis for the BDFRM and BDFIM, is a very old machine. Papers outlining its basic principles appeared at the beginning of the last century [1–3]. The next step in the development of this machine did not occur until approximately 50 years later [4–6]. Essentially the two machine cascade system was collapsed into a single frame. The two variants developed, the BDFIM and the BDFRM, used the same stator but the BDFRM replaced a special cage rotor of the BDFIM with a reluctance one.

In the last 10 years there has been a renewed interest in the BDFIM and the BDFRM due to the slip recovery nature of their operation. This means that if the speed range of operation is limited about a "synchronous" speed, then the inverter can be fractionally rated. Even though the machine needs to be larger for a given torque output, this fact means that the total system cost may be lower.

In many respects the BDFRM and the BDFIM are very similar, however the BDFRM has the potential for greater efficiency (since the rotor losses are much smaller than the BDFIM), and should be able to operate at higher speeds because the cageless rotor can be more robustly constructed. In addition, it is easier to model and control than the BDFIM.

BDFRM based drive technology may find application in such areas as turbo machinery (where the rugged nature of the rotor and the synchronous machine mode of operation can be exploited), variable speed constant frequency (VSCF) hydro and wind power applications, commercial heating and air conditioning, as well as in large pump drives.

The tendency of the BDFRM control literature [7–11] has been to focus on particular applications or control aspects, and not to carry out a complete parameter independent analysis of the machine. The purpose of this paper is to fill this void with a theoretical study of the following BDFRM control properties:

1. Conditions for maximum torque per secondary winding ampere.
2. Conditions for maximum torque per total primary and secondary winding amperes.
3. Power factor control and trade-offs with inverter volt-amperes.

II. Preliminaries

In the limited space available in this paper it is not possible to consider the detailed operation and modelling of the BDFRM. The interested reader is referred to [12, 13]. This section will therefore briefly present some definitions and expressions used in the remainder of the paper.

Fig. 1 shows the basic structure of the BDFRM. As can be seen, the machine logically has two windings wound on the same stator. The primary winding is connected to the grid,[1] and the secondary to an inverter. These two windings always have *different pole numbers*, and therefore with a round rotor there ideally wouldn't be any magnetic coupling between them. However, if the number of *salient rotor poles*, denoted by p_r, satisfies the following condition:

$$p_r = p_p + p_s \tag{1}$$

where p_p and p_s are the primary and secondary winding *pole pairs* respectively, then there is coupling between the windings. It can be shown that the degree of coupling is dependent on the rotor angle. This implies that there must be a change of co-energy with the rotor movement, and the machine can consequently develop torque. The other key relationship that must exist for a resultant torque to be produced is [12, 13]:

$$\omega_r = p_r \omega_{rm} = \omega_p + \omega_s \tag{2}$$

where $\omega_r \triangleq$ the electrical angular velocity of the rotor; $\omega_{rm} \triangleq$ mechanical angular velocity; $\omega_p \triangleq$ the supply frequency of the primary winding (rad/s); and $\omega_s \triangleq$ the supply frequency of the secondary winding (rad/s).

It is beyond the scope of this paper to develop the complete space vector model of the BDFRM, and relevant expressions, in

R.E. Betz is with the Department of Electrical and Computer Engineering, University of Newcastle, Callaghan, NSW, 2308, Australia. (e-mail: reb@ecemail.newcastle.edu.au)

M.G. Jovanović is with the School of Engineering, University of Northumbria at Newcastle, Newcastle upon Tyne NE1 8ST, United Kingdom. (e-mail: milutin.jovanovic@unn.ac.uk)

[1]The fact that the primary winding is connected to a constant voltage and frequency supply means that the primary flux linkage is constant.

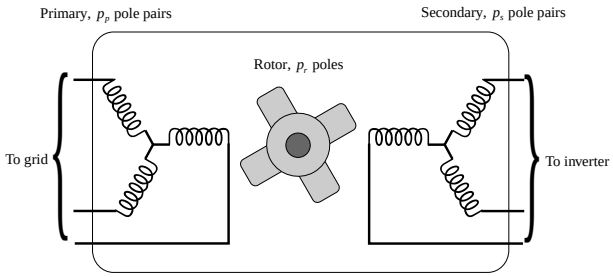

Fig. 1. Conceptual diagram of the BDFRM

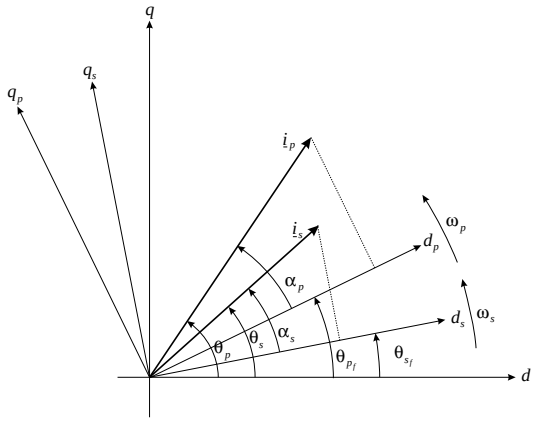

Fig. 2. The reference frames and current angles used for the BDFRM (*dq* frame is stationary).

a general reference frame rotating at ω, will simply be stated [9, 12, 13]:

$$\underline{v}_{p_r} = R_p \underline{i}_{p_r} + \frac{d\underline{\lambda}_{p_r}}{dt} + j\omega \underline{\lambda}_{p_r} \tag{3}$$

$$\underline{v}_{s_r} = R_s \underline{i}_{s_r} + \frac{d\underline{\lambda}_{s_r}}{dt} + j(\omega_r - \omega) \underline{\lambda}_{s_r} \tag{4}$$

$$\underline{\lambda}_{p_r} = L_p \underline{i}_{p_r} + L_{ps} \underline{i}^*_{s_r} \tag{5}$$

$$\underline{\lambda}_{s_r} = L_s \underline{i}_{s_r} + L_{ps} \underline{i}^*_{p_r} \tag{6}$$

where $L_p \triangleq$ the primary inductance, $L_s \triangleq$ the secondary inductance and $L_{ps} \triangleq$ the primary to secondary mutual inductance. The space vector notation used is as follows: $\underline{x}_{p_r}$ and $\underline{x}_{s_r}$ denote generic space vectors, $\underline{x}$, for the primary and secondary respectively in a rotating reference frame.

Remark 1: One of the most distinguishing features of the space vector equations for the BDFRM is that (3) and (4) are in two different reference frames – (3) is in the ω reference frame, and (4) is in the $\omega_r - \omega$ frame.

If one integrates (2) then a similar relationship between the reference frame positions for the primary and secondary windings (denoted by the sub-subscript "f" in Fig. 2) can be obtained:

$$\theta_{r_f}(t) = p_r \theta_{rm}(t) = \theta_{p_f}(t) + \theta_{s_f}(t) \tag{7}$$

The angles defined in Fig. 2 are used later in the paper.

Remark 2: The equations for the flux expressions are a little confusing at first sight. Consider (5) for example. This expression appears to contain currents in the primary reference frame (i.e. $\underline{i}_{p_r}$) as well as currents in the secondary reference frame (i.e. $\underline{i}^*_{s_r}$). However, $\underline{i}^*_{s_r}$ is a referred secondary current (but in a frequency not turns ratio sense) to the primary reference frame, and its components appear as AC quantities of $\omega_r - \omega_s - \omega = \omega_p - \omega$ angular frequency. This is the same frequency as the primary reference frame quantities with respect to the ω reference frame. Therefore the components of the $\underline{i}^*_{s_r}$ vector are the same as those of the complex conjugate of the secondary current, *but they are in the primary flux reference frame*. Note however that the referred and original current vectors rotate at different velocities with respect to the stationary frame - the referred vector at $\omega_r - \omega_s = \omega_p$ and the original one at ω_s. Similarly $\underline{i}^*_{p_r}$ in (5) is a referred primary current rotating at $\omega - \omega_p$ in the secondary reference frame [12]. The terms $L_{ps}\underline{i}^*_{s_r}$ and $L_{ps}\underline{i}^*_{p_r}$ can be interpreted as representing the mutual flux that is linking the two windings via the modulating action of the rotor. It is this modulating influence of the rotor on the stator mmfs that results in the previously mentioned frequency conversion.

If we choose the reference frame angular velocity, ω, to be the primary frequency, ω_p, then given (2), the original voltage equations (3) and (4) become:

$$\underline{v}_{p_r} = R_p \underline{i}_{p_r} + \frac{d\underline{\lambda}_{p_r}}{dt} + j\omega_p \underline{\lambda}_{p_r} \tag{8}$$

$$\underline{v}_{s_r} = R_s \underline{i}_{s_r} + \frac{d\underline{\lambda}_{s_r}}{dt} + j\omega_s \underline{\lambda}_{s_r} \tag{9}$$

Using a change of field energy technique, it is possible to derive a number of different expressions for the torque of the BDFRM [12]. The most important one for this paper is:

$$T_e = \frac{3}{2} p_r \frac{L_{ps}}{L_p} (\lambda_{pd} i_{sq} + \lambda_{pq} i_{sd}) \tag{10}$$

where the dq components are with respect to the primary and secondary reference frames, the p or s subscript denoting the particular frame.

Remark 3: Equations (8) and (9) are in their "natural" reference frames, with the primary equation in the ω_p frame, and the secondary equation in the ω_s frame. Remark 2 still holds in this new reference frame with the exception that the secondary currents are no longer AC but DC, and as such are much easier to control.

Remark 4: Equations (8) and (9) are of the same form as the equations for the double fed slip ring induction machine (DFSRIM). This, at first, is a little surprising given the different underlying operation principles of the two machines. It should be noted that the dynamics of the BDFRM are not as fast as those of the DFSRIM because of the higher leakage inductances.

Remark 5: Equation (10) is very similar to the dq expression for the torque of the induction machine with rotor flux orientation. This again serves to highlight the close connections between the two machines.

The other main property of the BDFRM that is of interest is its power. The standard space vector power expression [14] has been be used to derive the PU power expressions in Appendix-A.

III. Control Properties

The subsequent analysis assumes an ideal machine without saturation. In addition, in most cases, the stator resistance is

ignored in order to simply the development of the analytical expressions. This approximation should have little effect on the accuracy of the analysis. For simplicity the primary and secondary windings are assumed to have the same number of effective turns per pole i.e. the same inductances ($L_p = L_s$).[2]

A. Maximum Torque Per Secondary Ampere

A desirable property for a BDFRM is to maximise the torque produced for a given inverter current rating – i.e. maximise the torque per secondary ampere (MTPSA). Using (10) and aligning the reference frame with the primary flux vector (which effectively means that $\lambda_{pq} = 0$ and $\lambda_{pd} = \lambda_p$), the torque can be written as:

$$T_e = \frac{3}{2} p_r \frac{L_{ps}}{L_p} \lambda_p i_{sq} \tag{11}$$

Remark 6: The primary flux frame alignment used in (11) makes it obvious that one can control the torque in the BDFRM independently from the flux. λ_p is fixed by the grid supply voltage and frequency applied to the primary winding, and the torque is controlled by the secondary winding q axis current (i_{sq}).

From Fig. 2 one can see that $i_{sq} = i_s \sin\alpha_s$, and consequently the torque per secondary ampere can be written as:

$$\frac{T_e}{i_s} = \frac{3}{2} p_r \frac{L_{ps}}{L_p} \lambda_p \sin\alpha_s \tag{12}$$

which is clearly a maximum when $\alpha_s = \pi/2$.

Remark 7: Examination of (12) indicates that the torque per secondary ampere improves with increasing the L_{ps}/L_p ratio. It can be shown that this implies a larger saliency ratio for the rotor [15]. Therefore, the machine should be designed with the highest possible rotor saliency. The use of an axially-laminated rotor would be a preferable solution from this point of view, but it would also have high iron losses and be costly and difficult to manufacture. Recent radial laminated flux barrier rotor designs have nearly the same saliency ratio of the axially laminated design, are economic to manufacture, and have low iron losses [16, 17].

Remark 8: Note that this control strategy only minimises the secondary current – no consideration has been given to the current or the power factor of the grid connected (primary) winding.

B. Maximum Torque Per Total Amperes

An alternative strategy for controlling the BDFRM may be the maximum torque per total amperes (MTPTA) of the machine. The total amperes refers to the sum of the primary and secondary current magnitudes. In other words this strategy is essentially trying to share the current more evenly between the windings for a given torque output.

The problem to be solved can be stated mathematically in normalised terms as[3]:

$$\min_{\alpha_s,\alpha_p} i_{tn} = i_{pn} + i_{sn} = \frac{\zeta \sin\alpha_p + \sin\alpha_s}{\sin(\alpha_s + \alpha_p)} \tag{13}$$

[2]This choice of inductances may not be optimal in the sense of obtaining the maximum torque for a given amount of active copper and iron in the machine.

[3]ζ is defined in Appendix-A.

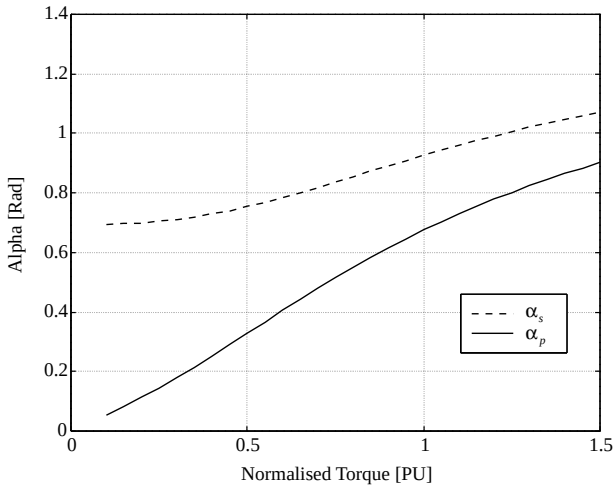

Fig. 3. α_s and α_p angles for maximum torque per total amperes.

subject to a specific torque output T_n.

Remark 9: The α_s and α_p variables in (13) are not independent due to the primary flux frame alignment condition implicit in (13) [18].

Equation (13) can, after considerable manipulation, be put into the following form [18]:

$$i_{tn} = \frac{\zeta T_n \sqrt{1 + \tan^2\alpha_s} + \sqrt{(2\tan\alpha_s - T_n)^2 + T_n^2 \tan^2\alpha_s}}{2\tan\alpha_s} \tag{14}$$

Theoretically one can differentiate (14) with respect to $\tan\alpha_s$, and then equate the obtained expression to zero to solve for the $\tan\alpha_s$ that will minimise i_{tn}. However, in practice the resultant derivative expression is very complex and cannot be solved analytically. Therefore the optimal angles have been calculated using a numerical minimisation procedure.

The plots developed from (14) are for the case where $L_p = L_s$ and the rotor has an equivalent synchronous reluctance machine saliency ratio of $\xi = L_d/L_q = 8$, which can be shown to be equivalent to $\zeta = 9/7$ [15, 18]. The plots are all developed for $\omega_{sn} = 1$ and torque levels ranging from 0.1-pu to 1.5-pu.

Fig. 3 shows the current angles required to achieve MTPTA operation.

Remark 10: One interesting feature of Fig. 3 is that α_s does not change as much as α_p. In addition the α_s angles are larger as compared to α_p for all the torque levels. This result is expected as the primary winding is mainly responsible for the machine magnetisation as opposed to the secondary which is torque producing. One can see from the same figure that at the low torques the primary angle approaches zero, indicating that it is supplying almost all the flux for the machine. The angle of the secondary current in this torque region, at first, would seem to indicate that it is also supplying significant flux to the machine. However, as we shall see in a subsequent plot the magnitude of i_{sn} approaches zero under these conditions. One could anticipate that this would be the case from (12).

Remark 11: The values of the individual winding current magnitudes can be found from (20) and (21). Notice that i_{pn} and i_{sn} don't explicitly contain the torque level T_n. However, as T_n varies, the α_s and α_p vary as illustrated in Fig. 3.

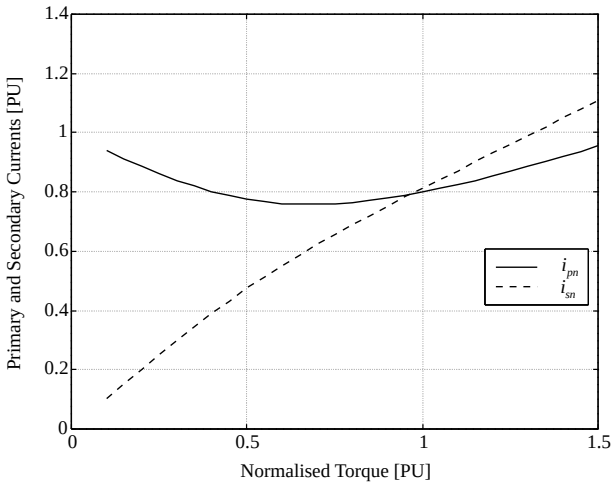

Fig. 4. Current magnitude components under maximum torque per total amperes.

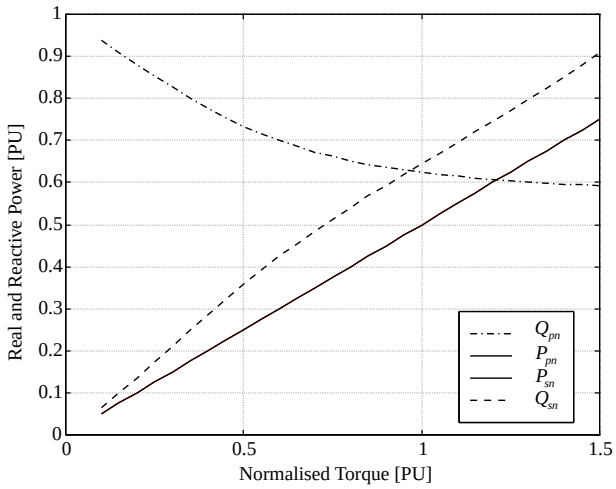

Fig. 5. Real and reactive powers under the maximum torque per total amperes condition with the secondary winding being supplied at the mains frequency (note that the real power of the windings is the same as $\omega_{sn} = 1$).

It would be instructive to break down the total current magnitude into its primary and secondary components under this condition. Fig. 4 shows the individual current magnitudes.

Remark 12: Fig. 4 demonstrates that the change in the total current magnitude, with respect to torque, largely results from the variation in the magnitude of the secondary current component. This is not unexpected, since from (11) one can see that the torque is directly related to the secondary q axis current. From Fig. 3 it is evident that α_s does not change a lot with torque, therefore the i_{sn} must be changing to effect the increased i_{sqn} component and hence torque output (see (19)).

Remark 13: The other relevant remark about Fig. 4 is that the primary current magnitude is relatively constant with torque variations. From Fig. 3 one can see that α_p increases considerably with increased torque, therefore one would conclude that the primary current is contributing less to the primary flux with rising torque levels, as opposed to the secondary current which is increasing its contribution to the flux (since λ_p is constant).

The statements in Remark 13 lead naturally to consideration of the power components for the primary and secondary windings. Fig. 5 shows these components under the MTPTA condition, developed using (24)–(27).

Remark 14: Examination of Fig. 5 sheds extra light on the comments in Remarks 12 and 13. One important observation is that the real power contributed by the primary and secondary windings are the same. This is a consequence of the $\omega_{sn} = 1$ assumption as follows from (24) and (26). If $\omega_{sn} < 1$ then the power contributed by the secondary winding becomes less. At the extreme, if $\omega_{sn} = 0$ (i.e. DC) then the secondary power is zero, since the secondary winding is now simulating the field winding of a classical synchronous machine.[4]

Remark 15: The reactive powers in Fig. 5 show that the primary reactive power decreases with increased torque, this indicating that the primary winding is participating less in the flux production (as noted earlier). On the other hand, one can see that the opposite occurs for the secondary winding, with the corresponding reactive power increasing significantly with increased torque.

[4]Note that under this condition there will be enough real power to supply the resistive losses of the winding. This does not show up in the analysis since we are neglecting resistances.

C. Power, Power Factor and Volt-Amperes

In order to understand the power relationships for the BDFRM we shall look at the power performance of the machine under constant torque and constant secondary frequency.

Consider (19), which we can rearrange to give:

$$F(\alpha_p, \alpha_s) = 2 \sin \alpha_s \sin \alpha_p - T_n \sin(\alpha_p + \alpha_s) = 0 \quad (15)$$

If we choose a value of α_s in (15) then we can solve for α_p for a specific value of T_n. In the following analysis we shall assume that the torque level is $T_n = 1$ and the secondary frequency is $\omega_{sn} = 1$. At the end of this section we shall briefly discuss what happens to the results as the torque and frequency are varied from these values.

The α_p and α_s profile resulting from (15) can be used to generate the magnitudes of the primary and secondary currents. This analysis gives one a good feel for the trade-offs that occur in relation to the inverter size to achieve particular power factor outcomes. Using (20) and (21) one can develop the plots shown in Figs. 6.

Examination of Fig. 6 immediately reveals that i_{pn} is at a minimum when $\alpha_s \approx 0.46$ radian. This point corresponds to the angle when the secondary winding is developing all the primary flux for the machine (via the mutually coupled flux), which in turn implies the $\alpha_p = \pi/2$. This means that the primary current is orthogonal to λ_p, and hence the primary current by itself does not produce any flux. One can see from Fig. 6 that the i_{pdn} component of the current is zero at this angle, further confirming the analysis. The other relevant aspect of the figure is that i_{pqn} is constant over the whole range of α_s angles. This is the component of the primary current that is in quadrature with λ_p, and therefore is the torque producing component i.e. the coupled secondary q axis current [18]. Given that ω_{pn} is fixed by the winding grid connection, the real power contributed by the primary is constant too.

Fig. 6 also shows the secondary current components. The

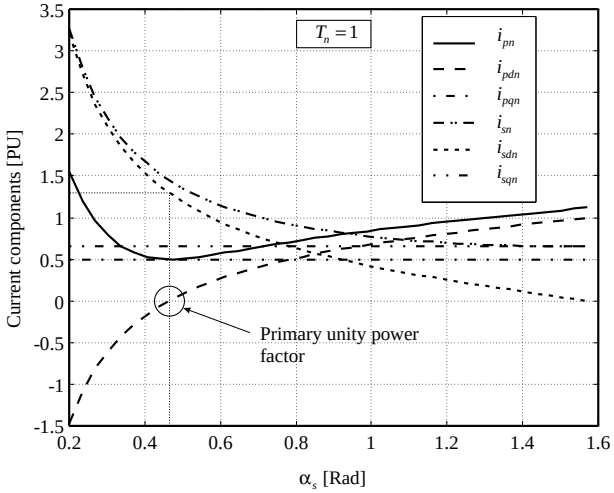

Fig. 6. Primary and secondary currents, $T_n = 1$ and $\omega_{sn} = 1$.

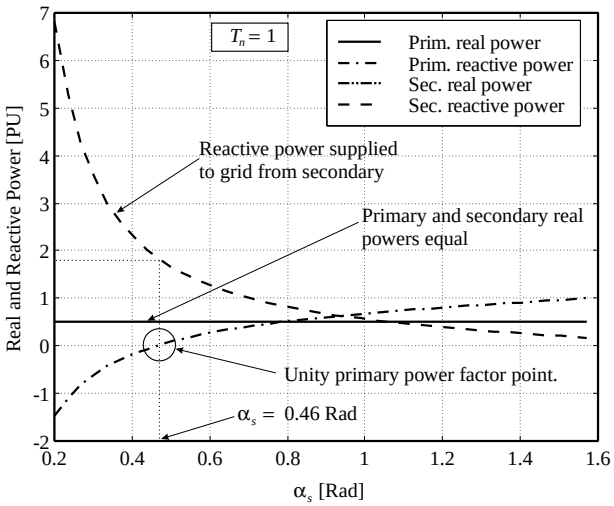

Fig. 7. Primary and secondary real and reactive powers, $T_n = 1, \omega_{sn} = 1$.

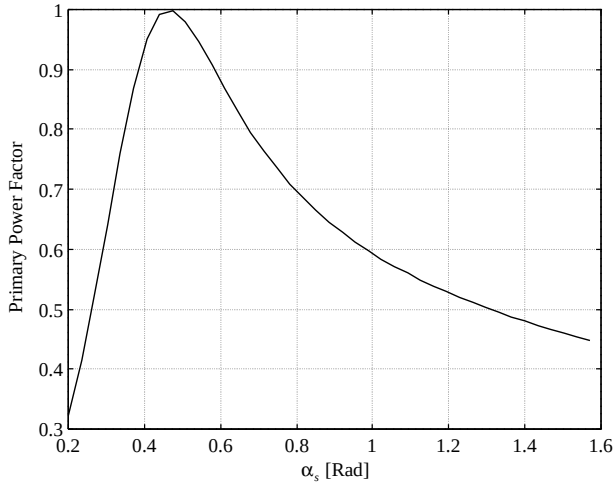

Fig. 8. Primary winding power factor when $T_n = 1$ and $\omega_{sn} = 1$.

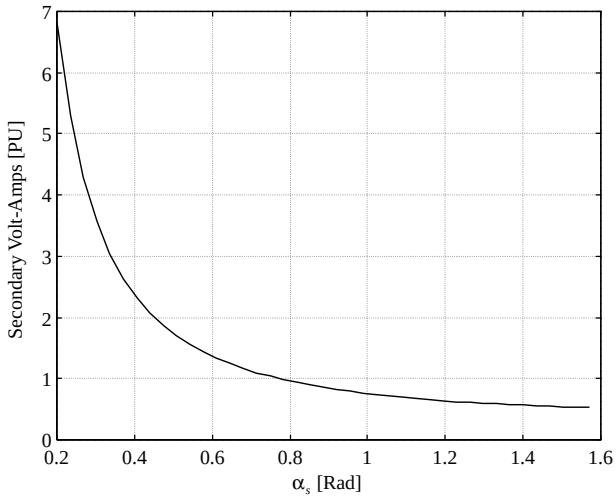

Fig. 9. Secondary winding volt-amperes (VA) with $T_n = 1$ and $\omega_{sn} = 1$.

most significant feature is the very high secondary current magnitude for low values of α_s. One can see that most of the increase in i_{sn} is due to the increase of the flux producing i_{sdn} component. For very small angles of α_s the machine can become over-excited and the primary winding begins to look capacitive. Notice, similarly to the primary winding, that the q axis component (i_{sqn}) of the current remains constant over the whole angle range.

Fig. 7 shows the power components under the same condition as Fig. 6.

Remark 16: In Fig. 7 note that the power factor of the primary is unity when $\alpha_s = 0.46$ radian and that the real power component of the primary winding is constant.

Remark 17: Fig. 7 graphically shows the significant change in the reactive power supplied by the secondary winding when $\alpha_s < 0.46$ radian. As $\alpha_s \to \pi/2$ then the reactive power of the secondary also approaches zero but does not reach zero at $\alpha_s = \pi/2$. This is due to the fact that the secondary reference frame is out of alignment with the secondary flux, therefore there is still a secondary flux producing component of current with $i_{sdn} = 0$.

One of the most interesting properties of the BDFRM is the ability to control the power factor of the primary via the secondary winding currents. Fig. 8 shows the primary power factor. This plot shows that the power factor of the primary does indeed become zero at $\alpha_s = 0.46$ radian. If one plotted the secondary power factor one would find that it is very poor for $\alpha_s \approx 0.3$, monotonically increasing with α_s, and nearly reaching one at $\alpha_s = \pi/2$.

The comments in the previous paragraph are further reinforced if one examines the volt-amperes (VA) absorbed by the secondary windings under the $T_n = \omega_{sn} = 1$ condition. Fig. 9 shows the secondary VA.

The discussion thus far has concentrated on the trade-offs associated with the control of the primary imaginary (or reactive) power. However, in the power plots one can notice that the real power delivered by the primary and secondary are equal (under the $\omega_{sn} = 1$ condition). If one examines (26) one can see that for a given non-zero torque the real power delivered by the secondary is related to the applied secondary frequency, whereas the real power delivered by the primary is independent of the secondary frequency (see (24)). If $\omega_{sn} > 1$ in (26) (i.e. high speed operation) then the real power contributed by the secondary will be greater than that of the primary, else (for

$\omega_{sn} < 1$) it is less. Clearly if $\omega_{sn} = 0$ then the secondary power is zero and the BDFRM operates as a synchronous machine.

If the phase sequence is reversed then $\omega_{sn} < 0$. This allows the machine to operate at sub-synchronous speeds i.e. at $\omega_{rm} < \omega_p/p_r$. If one considers (26) one can see that negative ω_{sn} corresponds to a negative P_{sn}. Therefore power is being regenerated from the secondary back into the supply. Note that in this mode the inverter must be capable of regeneration for sustained operation. When operating at speeds below synchronous speed the machine is very inefficient since energy is being taken from the supply via the primary, and then returned to the supply via the secondary. Therefore, some of the input energy is circulating from the primary to the secondary, incurring losses on the way.

All the previous plots were for the case of $T_n = 1$ and $\omega_{sn} = 1$. If these parameters are varied then the following further observations can be made. For the case of varying ω_{sn}:

- The real and imaginary current magnitudes flowing in the windings do not change.
- The current angle profile remains the same.
- As a consequence of the first two comments the maximum torque per total amperes does not vary.
- The *primary* real and imaginary powers are secondary frequency independent and therefore are unaffected by its variations.
- The *secondary* real and imaginary powers, and VA decrease at all α_s angles in proportion to ω_{sn}.
- Under the $\omega_{sn} = 0$ condition the α_s angle effectively becomes the torque angle of a synchronous machine. It corresponds to the initial phase of the secondary current relative to the secondary reference frame (which is now stationary). The latter is initially aligned with the high permeance axis of the rotor.

If the torque level is varied at $\omega_{sn} = 1$, then the following observations can be made:

- The primary and secondary current angles both approach zero as $T_n \to 0$.
- The real power is still evenly shared between the primary and secondary windings.
- The α_s versus α_p current angle profile changes with variations in T_n.
- The optimal torque per total amperes change, although only by a small amount.

D. Control Scheme

The BDFRM can be configured into a drive system employing vector control techniques [10, 11]. In case of primary flux orientation discussed previously, then a drive control system of the form of Fig. 10 can be devised.[5] As the secondary winding quantities are only controllable, the secondary reference frame position, θ_{s_f}, should be determined for control implementation. This can be achieved using the primary frame position, θ_{p_f}, (which is the same as the primary flux angle due to the alignment condition and can be therefore estimated from the measured grid voltages[6]), rotor position measurement, θ_{rm_f}, and (7). The desired inputs to the dq current controllers depend on a control strategy to be implemented. For example, if the maximum torque per secondary ampere strategy is of interest, then i^*_{sd} and i^*_{sq} is determined from (11) for a given torque command T^*_e.

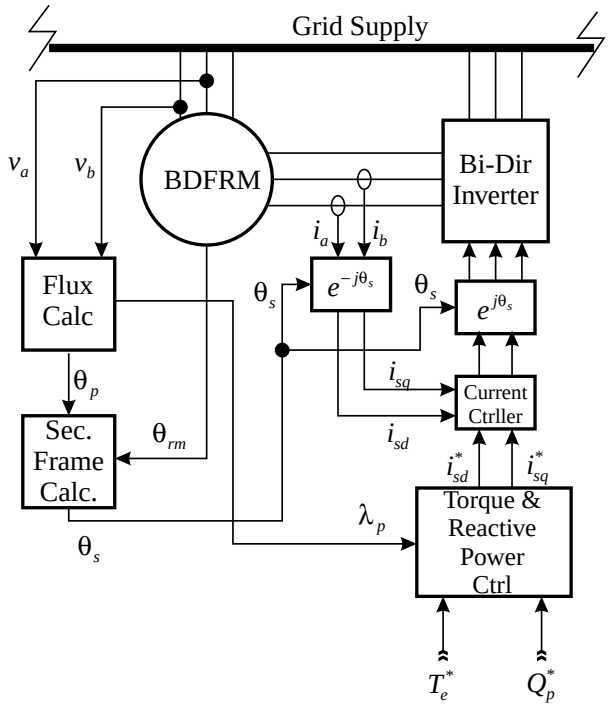

Fig. 10. Block diagram of a BDFRM based drive system.

IV. Conclusions

This paper has presented a number of properties of the BDFRM. The main feature of the machine is that it allows a smaller inverter to be used if the output speed range required is relatively small. However, as has been shown in the analysis above, if one utilises the ability of the inverter to control the primary winding power factor, then the inverter size has to increase, the amount dependent on the power factor one wishes to obtain.

In addition to the machine attributes examined, the paper has also introduced a number of per-unit (PU) based model equations for the BDFRM.

To summarise, the main conclusions that can be drawn from the paper are:

1. The maximum torque per secondary ampere (MTPSA) is achieved if $\alpha_s = \pi/2$. This angle is independent of the applied secondary frequency and the torque level.
2. If the machine is operated with $\alpha_s = \pi/2$, the primary power factor is poor (i.e. ≈ 0.47). In many applications this may not be satisfactory.
3. The maximum torque per total amperes (MTPTA) current angles for the BDFRM do not equal the MTPSA current angle. Furthermore, the MTPTA angles are dependent on the torque level that the machine is operating at.

[5] Fig. 10 does not show the circuitry required for starting the system. If a partially rated inverter is used then an auxiliary contactor is usually required to short the secondary. This allows the machine to start as an induction machine. Once the machine is near the synchronous speed the contactors are opened and the inverter is connected.

[6] Estimation errors can occur by ignoring the primary winding resistance, but in most cases this error is negligible because of fi xed 50-Hz supply.

4. The paper has highlighted the implications of primary power factor control on the rating of the secondary winding inverter.

The analysis in this paper, due to space restrictions, is necessarily limited. Nevertheless, it indicates that the BDFRM has many interesting properties that can be potentially utilised in many applications. The authors believe that the BDFRM deserves more investigation to determine whether it is industrially viable in the target applications.

APPENDIX

A. Normalised Parameters

It is possible to derive a set of per-unit bases for the BDFRM corresponding to an arbitrarily chosen $\alpha_s = \alpha_p = \pi/4$ current angle condition [18]:

$$T_B = \frac{3}{4} p_r \frac{\lambda_p^2}{L_p}; \qquad P_B = \frac{2\omega_B}{p_r} T_B \tag{16}$$

$$i_B = \frac{\lambda_B}{L_B} = \frac{\lambda_p}{L_p}; \qquad \lambda_B = \frac{v_B}{\omega_B} = \lambda_p \tag{17}$$

$$\omega_B = \omega_p = 2\pi f_B; \qquad L_B = L_p \tag{18}$$

where v_B and f_B are the grid supply voltage and frequency.

These base values can be used to convert the main performance equations into the normalised forms that appear below:

$$\text{Torque: } T_n = \frac{2\sin\alpha_s \sin\alpha_p}{\sin(\alpha_p + \alpha_s)} = \frac{2}{\zeta} i_{sn} \sin\alpha_s \tag{19}$$

$$\text{Primary current: } i_{pn} = \frac{\sin\alpha_s}{\sin(\alpha_p + \alpha_s)} \tag{20}$$

$$\text{Secondary current: } i_{sn} = \frac{\zeta \sin\alpha_p}{\sin(\alpha_p + \alpha_s)} \tag{21}$$

$$\text{Primary flux: } \lambda_{pn} = 1 \tag{22}$$

$$\text{Secondary flux: } \underline{\lambda}_{sn} = L_{sn}\underline{i}_{sn} + \frac{1}{\zeta}\underline{i}^*_{pn} \tag{23}$$

The PU real and reactive power expressions are:

$$P_{pn} = \frac{1}{\zeta} i_{sn} i_{pn} \sin(\alpha_s + \alpha_p) = \frac{\sin\alpha_p \sin\alpha_s}{\sin(\alpha_s + \alpha_p)} = \frac{1}{2} T_n \tag{24}$$

$$Q_{pn} = 1 - \frac{i_{sdn}}{\zeta} = \frac{\sin\alpha_s \cos\alpha_p}{\sin(\alpha_s + \alpha_p)} \tag{25}$$

$$P_{sn} = \frac{1}{\zeta} \omega_{sn} i_{sn} i_{pn} \sin(\alpha_s + \alpha_p) = \frac{\omega_{sn}}{2} T_n \tag{26}$$

$$Q_{sn} = \frac{\omega_{sn} \sin\alpha_p}{\sin^2(\alpha_s + \alpha_p)} [\frac{\sin\alpha_p}{k_{ps}^2} + \sin\alpha_s \cos(\alpha_s + \alpha_p)] \tag{27}$$

where $\zeta = L_p/L_{ps}$ and $k_{ps} = L_{ps}/\sqrt{L_p L_s}$. The "$n$" subscripts denote that the relevant quantity is a PU or normalised quantity.

REFERENCES

[1] L. Hunt, "A new type of induction motor," *J. IEE*, vol. 38, pp. 648–667, 1907.

[2] L. Hunt, "The cascade induction motor," *J. IEE*, vol. 52, pp. 406–426, 1914.

[3] F. Creedy, "Some developments in multi-speed cascade induction machines," *J. IEE*, vol. 59, pp. 511–532, 1921.

[4] A. Broadway and L. Burbridge, "Self-cascaded machine: A low speed motor or a high frequency brushless alternator," *Proc. IEE*, vol. 117, pp. 1277–1290, July 1970.

[5] A. Broadway, "Cageless induction machines," *Proc. IEE.*, vol. 118, pp. 1593–1600, November 1971.

[6] A. Broadway, B. Cook, and P. Neal, "Brushless cascade alternator," *Proc. IEE*, vol. 121, pp. 1529–1535, December 1974.

[7] L. Xu, F. Liang, and T. Lipo, "Transient model of a doubly excited reluctance motor," *IEEE Trans. on Energy Conversion*, vol. 6, pp. 126–133, March 1991.

[8] L. Xu and Y. Tang, "A novel wind-power generating system using field orientation controlled doubly-excited brushless reluctance machine," *Proceeding of the IEEE IAS Annual Meeting*, pp. 408–418, 1992.

[9] Y. Liao, L. Zhen, and L. Xu, "Design of a doubly-fed reluctance motor for adjustable speed drives," *Proceedings of the IAS Annual Meeting*, vol. 1, pp. 305–312, Oct 1994.

[10] Y. Tang and L. Xu, "Vector control and fuzzy logic control of doubly fed variable speed drives with DSP implementation," *IEEE Trans. on Energy Conversion*, vol. 10, pp. 661–668, December 1995.

[11] L. Xu, L. Zhen, and E. Kim, "Field-orientation control of a doubly excited brushless reluctance machine," *IEEE Transactions on Industry Applications*, vol. 34, pp. 148–155, January/February 1998.

[12] R. Betz and M. Jovanović, "Introduction to brushless doubly fed reluctance machines - the basic equations," tech. rep., Dept. Elec. Energy Conversion, Aalborg University, Denmark., April 1998. Available at ftp://murray.newcastle.edu.au/pub/reb/Papers/BDFRMRev.pdf.

[13] F. Liang, L. Xu, and T. Lipo, "D-q analysis of a variable speed doubly AC excited reluctance motor," *Electric Machines and Power Systems*, vol. 19, pp. 125–138, March 1991.

[14] P. Vas, *Vector Control of AC Machines*. Oxford University Press, 1990.

[15] R. Betz and M. Jovanović, "The brushless doubly fed reluctance machine and the synchronous reluctance machine – a comparison," *Proceedings of the IEEE-IAS Annual Meeting*, Oct. 1999.

[16] A. Vagati and T. Lipo, eds., *Synchronous Reluctance Motors and Drives – a New Alternative*, IEEE Industry Applications Society, Oct 1994. Tutorial course presented at the IEEE-IAS Annual Meeting, Denver Colorado.

[17] A. Vagati, A. Canova, M. Chiampi, M. Pastorelli, and M. Repetto, "Improvement of synchronous reluctance motor design through finite-element analysis," *Conference Record of the 34th IEEE Industry Applications Society Annual Meeting*, vol. 2, pp. 862–871, Oct 1999.

[18] R. Betz and M. Jovanović, "Comparison of the brushless doubly fed reluctance machine and the synchronous reluctance machine," tech. rep., Department of Electrical Energy Conversion, Institute of Energy Technology, Aalborg University, Denmark, October 1998. Available at ftp://murray.newcastle.edu.au/pub/reb/Papers/bdfrm-sync.pdf.

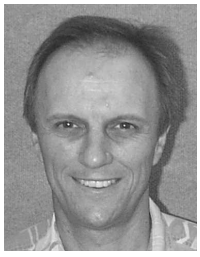

Robert E. Betz (M'92) received the B.E., M.E. and Ph.D. degrees from the University of Newcastle, Newcastle, Australia in 1979, 1982 and 1984 respectively. He is currently an Associate Professor in the Department of Electrical and Computer Engineering, University of Newcastle. His major interests are electrical machine drives, real-time operating systems, and industrial electronics. Dr. Betz is a member of the Industrial Drives Committee and Electric Machines Committee of the IEEE Industry Applications Society.

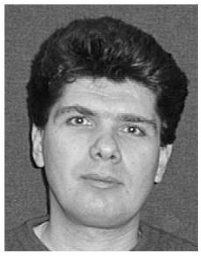

Milutin G. Jovanović received the Dipl.Eng and M.E.E. degrees from University of Belgrade, Belgrade, Yugoslavia, in 1987 and 1991 respectively, and the Ph.D. degree from the University of Newcastle, Newcastle, Australia, in 1997. He is currently a Senior Lecturer in the School of Engineering, University of Northumbria at Newcastle, UK. His main interests are in the areas of electrical machines and drives, power electronics and power systems. Dr. Jovanović is a member of the Electric Machines Committee and Industrial Drives Committee of the IEEE IAS.